Journal of Alloys and Compounds 768 (2018) 775–781

Contents lists available at ScienceDirect

Journal of Alloys and Compounds

journal homepage: http://www.elsevier.com/locate/jalcom

Fabrication of reinforced α+β titanium alloys by infiltration of Al into porous Ti-V compacts

Sumin Kim, Hwaebong Jung, Hyun Jun Rim, Hyun-Sook Lee**, Wooyoung Lee*

Department of Materials Science and Engineering, Yonsei University, 50 Yonsei-ro, Seodaemun-gu, Seoul, 03722, Republic of Korea

ARTICLE INFO

Article history:
Received 9 February 2018
Received in revised form
11 July 2018
Accepted 23 July 2018
Available online 27 July 2018

Keywords:
Titanium alloy
Alpha-beta phase
Intermetallic compounds
Powder injection molding
Infiltration
Mechanical property

ABSTRACT

We present an efficient process to fabricate reinforced titanium α + β alloys. Porous Ti compacts containing vanadium were prepared by a metal injection molding process. Infiltration of molten Al and subsequent heat treatments were performed to synthesize a variety of Ti-V-Al alloys. The V-added specimens showed better mechanical properties than those of V-free Ti-Al intermetallic compounds. Microstructural observation of the fracture surface revealed that the lamellar structure in the Ti-V-Al alloys plays an important role in improving their mechanical properties by postponing the propagation of cracks. Notably, the lamellar structures in the Ti-V-Al alloys disappeared and the mechanical properties deteriorated as the Al infiltration duration time increased. Therefore, Al infiltration time is a crucial factor for successful growth of well-defined lamellar structured α + β phases in Ti-V-Al alloys.

1. Introduction

Over several years, titanium and titanium-based alloys have been extensively utilized in the mainstream applications including the bio-medical, aerospace, and automotive industries, the reason being that the titanium is known to have high strength, good corrosion resistance, and low density (4.5 g/cm^3) [1–4]. Ti-based alloys are divided into three predominant groups: α, β, and α + β alloys. The specific phases are formed and stabilized depending on the content of the alloy elements.

As is well-known, alpha and near-alpha alloys such as Ti-5Al-2Sn and Ti-6Al-2Sn-4Zr-2Mo have promising strength, toughness, and creep resistance. Within the category of the α-stabilizers, there exist interstitial elements such as O, N, and C, but Al and Sn are also present and, are essential alloying elements for titanium alloys. Beta alloys possess good ductility and toughness, as well as low basic strength, but excellent formability can be retained upon cooling to room temperature. A drawback of the beta alloys is that α precipitations are formed during the cooling process, which can be impeded by fast cooling rates. However, when the sufficient β stabilizers are added to Ti composites, the beta alloys has an increased heat treatability, which allows remarkable strengthening to be achieved by controlling the decomposition of β-phase to α-phase during the heat treatment process. Representative β alloys include Ti-4.5Al-3V-2Fe-2Mo and Ti-5Al-4Mo-4Zr-2Sn-2Cr, with Mo, V, Nb, Ta, Fe, Cr, Ni, and Si functioning as the stabilizing elements. Alloys belonging to the α + β system can contain a number of α and β stabilizers, in which the β stabilizer(s) must be coupled with α soluble elements. These alloys can be strengthened by a solution treatment, which is typically performed at a temperature as high as in the two-phase field, followed by liquid quenching with water or another soluble quenchant. The alloys are then aged to precipitate α and yield a fine mixture of α and β in the retained or transformed β phase. By this route, Ti-6Al-4V, the most popular synthesized α + β alloy, is remarkably strengthened by the favorable properties of both α and β alloys (i.e., high strength and ductility along with good weldability and fabricability) [5–7].

In particular, in the research field of Ti-6Al-4V alloys, many efforts have been under way to enhance the mechanical properties by controlling the content of interstitial elements (O, C, N, and H), microstructure and texture. For this, several processes were introduced: i) solution treatment, quenching, and aging [8], ii) powder compact forging [9], iii) hydrogen sintering and phase

* Corresponding author.
** Corresponding author.
E-mail addresses: h-slee@yonsei.ac.kr (H.-S. Lee), wooyoung@yonsei.ac.kr (W. Lee).

https://doi.org/10.1016/j.jallcom.2018.07.263
0925-8388/

transformation [10], iv) hydrogenation-dehydrogenation treatment [11], v) laser solid forming [12], etc.

Ti-based alloys are usually fabricated using a conventional ingot metallurgy (IM) method. However, the IM method is relatively expensive compared with that used for steel and aluminum [13]. For such a reason, an intensive research was focused on lowering the cost of the process for the Ti-based alloys. In this vein, we employed a process which effectively incorporate favorable aspects of powder injection molding (PIM) and infiltration of second (Al) and/or third (Mg) elements to fabricate in-situ strengthened Ti composites, as reported in our previous study [9]. However, various phases such as pure Ti, Ti-Al intermetallic phase, and/or Al(Mg) alloy were in homoegeneously distributed in the Ti composites. Although post-heat treatment after infiltration successfully led to the formation of a uniformly distributed single phase, Ti_xAl_y, the heating process detrimentally degraded its mechanical properties relative to those of the as-infiltrated specimens. In this study, we suggest an efficient method to enhance the mechanical properties of Ti composites composed of a monolithic phase even after post-heat treatment. Specifically, vanadium was added to pure Ti and molten Al was infiltrated into the porous Ti-V compact, strengthened Ti $\alpha + \beta$ alloys were fabricated after subsequent heat treatments. The effects of V addition and Al infiltration on the mechanical properties of the vanadium-added specimens were analyzed by comparing their microstructural and compositional changes with the vanadium-free specimens.

2. Experiment procedures

The traditional powder metallurgy process of powder injection molding was used to prepare porous composites composed of titanium and vanadium. TiH_2 powders (>99%, −325mesh, SE-JONG) and vanadium powders (99.5%, −325mesh, Alfa Aesar) were used. The −325mesh TiH_2 powder has the particle size distribution of D10 = 4.829 μm, D50 = 18.850 μm, and D90 = 47.314 μm. The powders were mixed with the binders polypropylene (PP), polyethylene glycol (PEG) 20000, PEG 4000, and carnauba wax (CW). The initial powders (TiH_2:V) and binders (PP:PEG20000:-PEG4000:CW) were prepared in a ratio of 45:2 wt.% and 31:55:10:4 vol.%, respectively. The powders and binder were mechanically mixed in a ratio of 53:47 vol.% for 24 h using a V-mixer. As the content of TiH_2 powder increases, the viscosity of the powder-binder mixture increases. High viscosity leads to problems in the production of specimens in mold form during powder injection molding process. Conversely, low content of TiH_2 powder in the mixture cause defects such as crack and deformation during sintering. Therefore, we derived the optimal ratio of powder and binder by measuring density and viscosity according to the ratio. The mixture was compacted into a green preform, having the geometry and dimensions presented in Fig. 1(a), by an extrusion and injection molding process. Subsequently, the porous Ti specimens containing vanadium were obtained during heat treatment, which was performed to remove residual binders and decompose H_2 from TiH_2. The detailed procedure is described in our previous report [14]. Following this procedure, the specimen was sintered at an isothermal temperature of 1200 °C for 2 h under vacuum (~10^{-3} Pa). After sintering, the dimensions of the specimen shrank by 30% compared to the original mold. The resultant porosity was approximately 10%, as measured by a pore size analyzer (AutoPore IV 9500). The pores of the Ti-V compact were infiltrated with Al by immersion in a bath of molten Al at 730 °C for 5, 10, and 15 s under an Ar atmosphere. A schematic diagram of the experimental setup for immersing the porous Ti-V compact into the molten Al is shown in Fig. 1(b). After Al infiltration, solution treatment was performed at 1000 °C for 3 h, followed by water quenching; precipitation age hardening was then carried out at 550 °C for 24 h, followed by air cooling. The heat treatment cycles for solutionizing and aging are shown in Fig. 1(c).

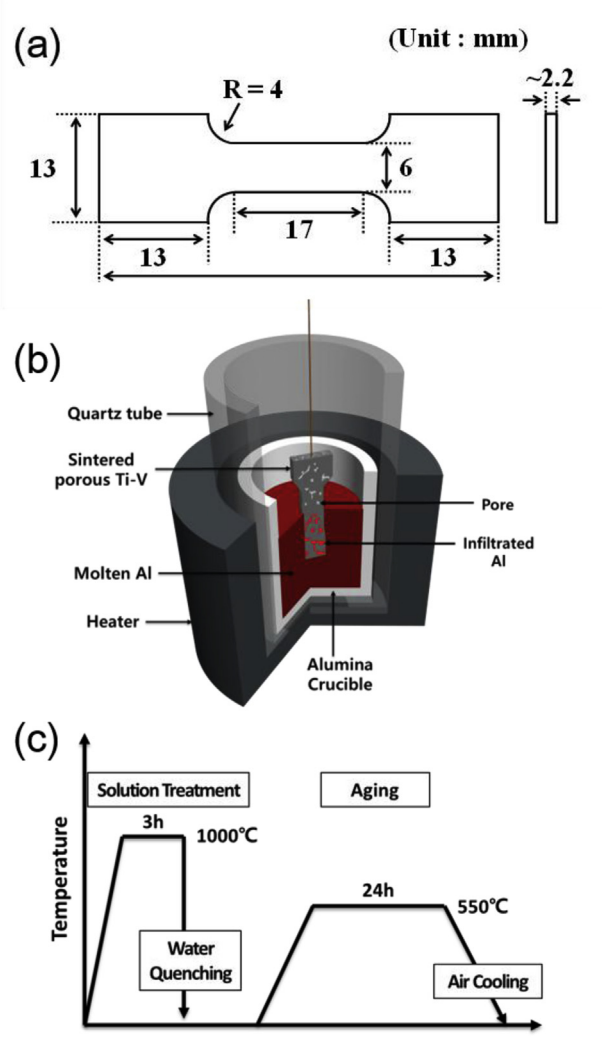

Fig. 1. (a) Geometry and dimensions of test pieces for tensile test, (b) schematics of fabrication process to infiltrate Al into pores in Ti-V, and (c) scheme of the heat treatment cycles applied in this study to fabricate the Ti-V-Al ($\alpha + \beta$) alloys.

To investigate the effect of vanadium in a Ti alloy, various Ti alloy specimens without vanadium were also prepared, including pure Ti, Al-infiltrated Ti, and post-heat treated Ti-Al alloys. The pure Ti sample was prepared by sintering the porous Ti specimen at 1200 °C for 2 h. The Al-infiltrated Ti was produced by infiltrating Al into the pores of pure Ti at 730 °C for 30s. The post-heat treated Ti-Al sample was fabricated after additional heating was performed on the Al-infiltrated Ti specimen at 1000 °C for 2 h to form a homogenous intermetallic phase between Ti and Al.

The constituent phases and their distributions were characterized using an X-ray diffractometer (XRD; Advanced LynxEye) with Cu K_α radiation and a field-emission scanning electron microscopy (FE-SEM, JEOL, JSM 7800F) equipped with an energy-dispersive X-ray spectroscopy (EDS). In order to investigate the mechanical properties of the Ti alloys, tensile tests were performed at room temperature at an initial strain rate of 1×10^{-4} s^{-1} using a servo hydraulic universal tensile testing machine (Instron, 3382). Subsequently, FE-SEM was used to observe the fractured surf aces of

the tensile specimens.

3. Results and discussion

The microstructures of the Ti-Al alloy (prepared by post-heat treatment after Al infiltration into pure porous Ti) and Ti-V-Al alloy (prepared by solution treatment and age hardening after Al infiltration into porous Ti-V) specimens were investigated with FE-SEM. The effect of subsequent heat treatment on the microstructures was also analyzed by comparison of the SEM images recorded with back-scattered electrons (BSE). The resultant SEM images of the Ti-Al and Ti-V-Al alloys are presented in Fig. 2(a) and (b), respectively, while Fig. 2(c) shows a magnified view of the latter alloy. As shown in the SEM images, the as-prepared specimens have different microstructures: many voids in the post-heat treated Ti-Al alloy (Fig. 2(a)) whereas lamellar structures, consisting of α-phase (gray region) and β-phase (white region) grain boundaries, in the Ti-V-Al alloy (Fig. 2(b) and (c)).

The crystal structures of post-heat treated Ti-Al alloy and Ti-V-Al alloy were characterized using XRD analysis. The XRD patterns are displayed in Fig. 3. The diffraction peaks were indexed to the crystal structures of hexagonal Ti_3Al (JCPDS: 14-0451) for the Ti-Al alloy (Fig. 3(a)) whereas hexagonal α-Ti (JCPDS: 44-1294) and cubic β-Ti (JCPDS: 44-1288) for the Ti-V-Al alloy (Fig. 3(b)). Secondary alloy phases were not observed within the limit of XRD resolution. In particular, the content of α and β phases of Ti-V-Al alloy was estimated by Rietveld refinement method using the XRD data in Fig. 3(b). As a result, the volume fractions of α and β phases were determined to be ~80.4 wt.% and ~19.6 wt.%, respectively, which are consistent with the results obtained from the SEM image analysis. The average area fractions of α and β phases were measured using five BSE-SEM micrographs included in Fig. 2(c), which were ~79.3 wt.% and 20.7 wt.%, respectively.

According to the results seen in Figs. 2(a) and 3(a), many voids are observed in the post-heat treated Ti-Al alloy grown with an intermetallic Ti_3Al phase. This is consistent with the result reported in our previous work [14], in which voids were inevitably formed in spite of homogenous growth of an intermetallic Ti_3Al phase. The generation of such voids can be explained in terms of: (i) the melting and/or evaporation of Al, (ii) the difference in molar volumes between the reactants and products, and (iii) the Kirkendall effect caused by the dissimilar diffusion rates of Ti and Al, as described in our previous study [14]. In this way, voids are evident in the post-heat treated Ti-Al alloy, as seen in Fig. 2(a). In contrast, substantially reduced number of voids are observed in the Ti-V-Al alloy grown with α and β phases that was produced by different heat treatments (solutionizing and aging) after Al infiltration for 5 s, as seen in Fig. 2(b).

In order to identify the phases of lamellar structures observed in the SEM images in Fig. Fig. 2(b) and (c), the compositional analysis was performed over the micro-scale range using the FE-SEM equipped with an EDS analyzer. Point EDS spectrum analysis was carried out at different locations where α and β phases are indicated in the SEM images of Fig. 4(a). The EDS spectra in Fig. 4(a) show that the contents of Al and V are observed to be different for the α and β phases: a higher amount of Al and a lower amount of V in the α-phase and a higher amount of V and a lower amount of Al in the β-phase. Two-dimensional EDS mapping was also performed on the same sample to investigate the elemental distribution as shown in Fig. 4(b). The mapping results are in agreement with the point scanning observation in Fig. 4(a), i.e. α-phase region is rich in Al whereas β-phase region is rich in V. The elemental distributions of Al and V in α and β phases of our Ti-V-Al alloy are found to be coincide with the results reported by other groups [15,16]. These results are attributed to the fact [17] that Al and V act as stabilizing elements for α and β phases, respectively.

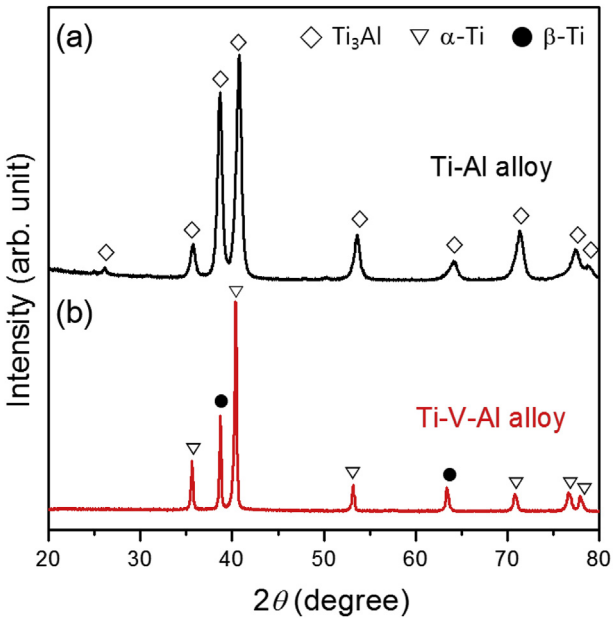

Fig. 3. XRD patterns of (a) post-heat treated Ti-Al alloy and (b) Ti-V-Al alloys.

In general, the phase of the as-quenched specimens after annealing above T_β can transform from β-phase to α′ martensite phase on quenching and can decompose to fine α and β-phases on aging [2,18,19]. To date, most studies involving solution treatment have been performed by isothermal annealing in the time range of 10 min to 1 h [2,18–22]. In this work, however, the isothermal annealing at temperatures above T_β was maintained for 3 h. The pores of the Ti-V composite have a high concentration of Al immediately after Al infiltration; hence, a prolonged annealing time was applied to diffuse Al into the entire specimen uniformly. The

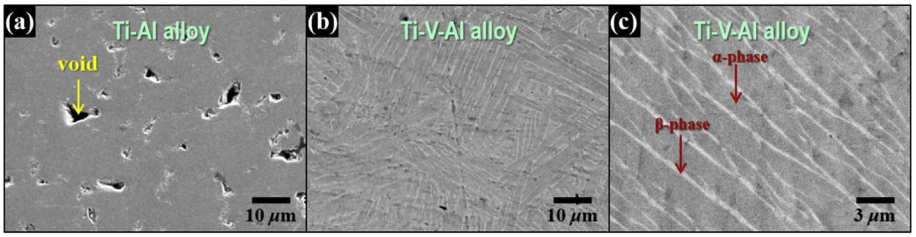

Fig. 2. SEM images of (a) post-heat treated Ti-Al alloy and (b) Ti-V-Al alloys. The (c) shows a magnified view of (b).

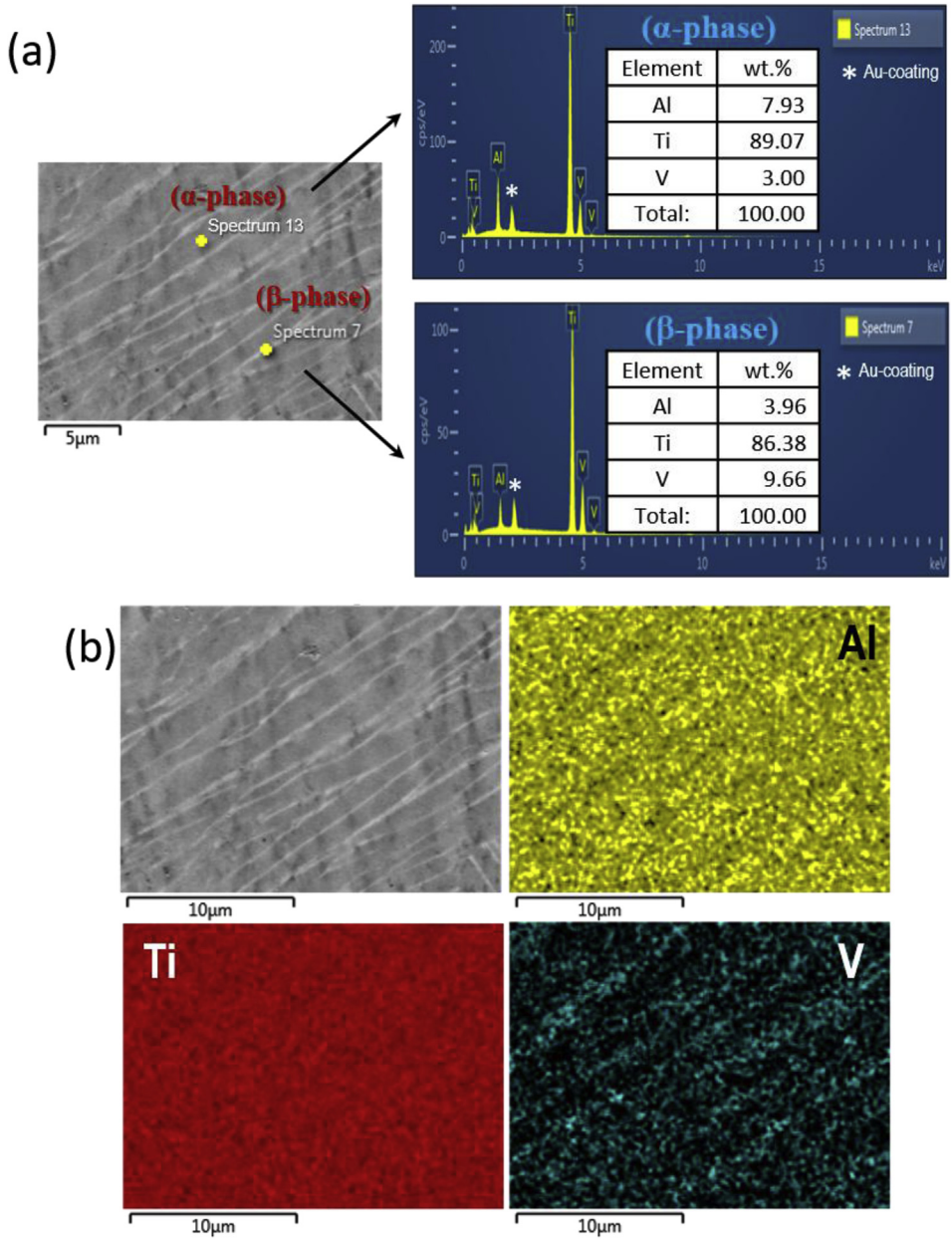

Fig. 4. SEM/EDS analysis of Ti-V-Al alloys. (a) EDS spectra obtained from a point analysis at different positions of α and β phases indicated in the SEM image and (b) SEM image depicting analyzed region and EDS elemental color mapping images for Al, Ti, and V. (For interpretation of the references to color in this figure legend, the reader is referred to the Web version of this article.)

uniformly distributed lamellar structures shown in the Ti-V-Al alloy reveal that solid-state diffusion was sufficiently achieved in the specimen.

The mechanical properties of various specimens of Ti-Al and Ti-V-Al alloys were examined by measuring tensile strength under a slow strain rate at room temperature. The tensile test results of the tensile stress–strain curves for the Ti-Al and Ti-V-Al alloys are exhibited in Fig. 5(a) and (b), respectively. As seen, the ultimate tensile strength (UTS) and elongation (EL) mechanical properties were profoundly enhanced. Fig. 5(a) presents the tensile stress–strain curves for various Ti-Al alloys, including pure Ti, Al-infiltrated Ti, and post-heat treated Al-infiltrated Ti. Pure Ti yields a UTS and EL of ~240 MPa and ~4.8%, respectively, whereas the UTS increases to 513 MPa and the EL reduces to 4.24% after Al infiltration. By the post-heat treatment, both the UTS and EL in the Ti-Al alloys depreciate considerably, which may be caused by growth of a brittle intermetallic phase and generation of many voids. On that account, it is clear that achieving a homogeneous phase through post-heat treatment to improve the mechanical properties of the alloy was unsuccessful. Fig. 5(b) shows the tensile stress–strain curves of Ti-V-Al alloys prepared with Al infiltration times of 5, 10, and 15 s. The highest tensile performance of UTS (~697 MPa) and EL (~7.39%) was found to occur for the Ti-V-Al alloy prepared with an infiltration time of 5 s. As the infiltration time increases, the mechanical properties are reduced: UTS of ~515 MPa and EL of ~6.75% for 10 s and UTS of ~334 MPa and EL of ~4.09% for 15 s.

To clarify the differences in the mechanical properties between

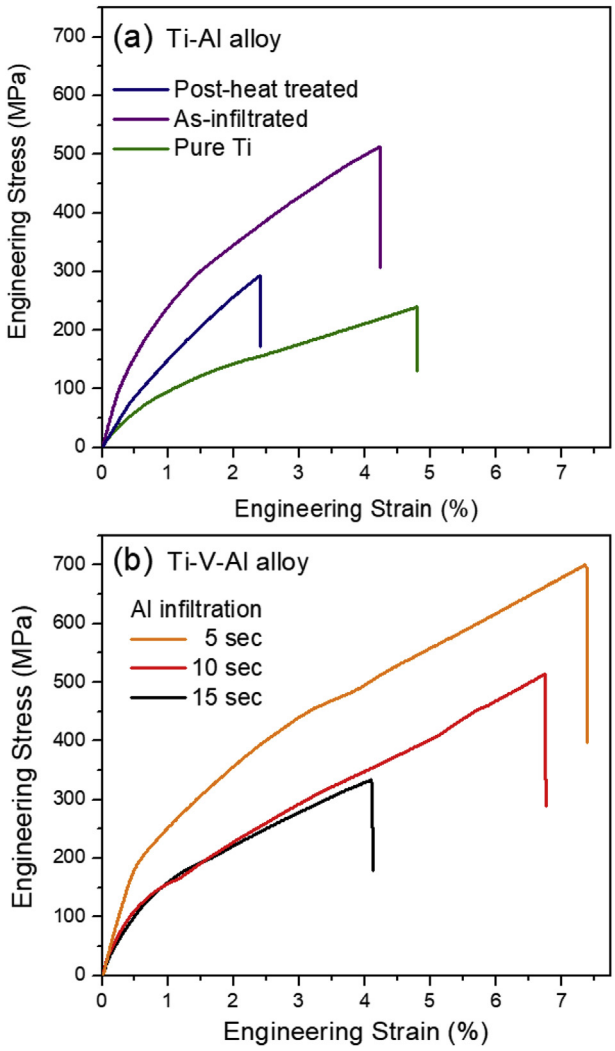

Fig. 5. Tensile engineering stress-strain curves of (a) various Ti-Al alloys and (b) Ti-V-Al alloys prepared with different Al infiltration times (5, 10, and 15 s).

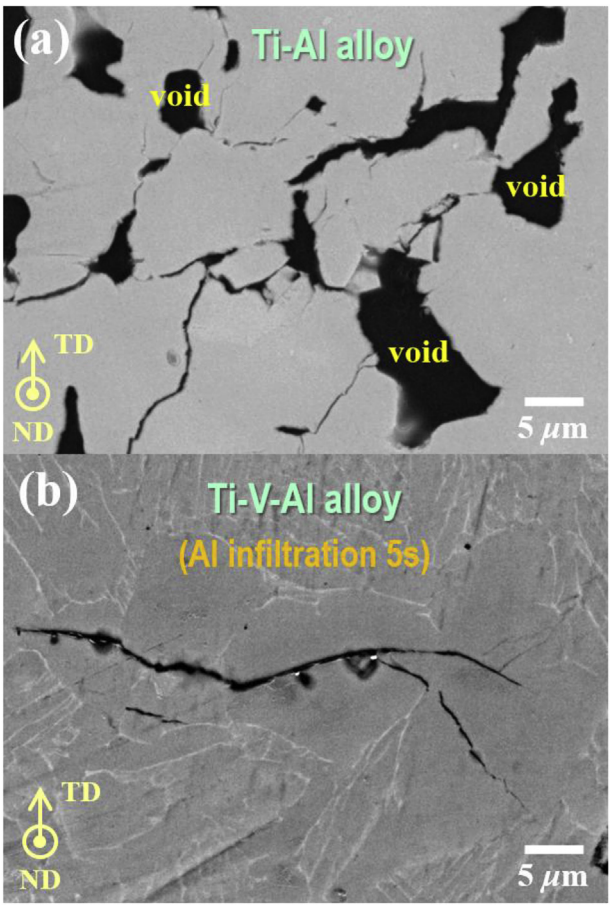

Fig. 6. SEM images of the fractured surface of (a) post-heat treated Ti-Al alloy and (b) Ti-V-Al alloy prepared with 5 s infiltration, which were observed at the normal direction (ND) perpendicular to the tensile direction (TD).

the Ti-Al intermetallic compounds and the Ti-V-Al ($\alpha + \beta$) alloys, the surfaces of fractured tensile specimens were observed along the normal direction (ND) perpendicular to the tensile direction (TD). Fig. 6 shows the SEM images of the fractured surface; specifically, Fig. 6(a) shows the Ti-Al alloy prepared after post-heat treatment, and Fig. 6(b) shows the Ti-V-Al ($\alpha + \beta$) alloy prepared after solutionizing and aging. As seen in Fig. 6(a), numerous cracks are formed along the voids of the Ti-Al intermetallic compound. This indicates that voids are one of the main causes of mechanical property degradation of Ti-Al intermetallic compounds. By comparison, few cracks are observed in the vicinity of the fractured area in the $\alpha + \beta$ phases, as seen in Fig. 6(b). In particular, cracks within the Ti-V-Al ($\alpha + \beta$) alloys propagate along the α-phase and avoid the lamellar structure. Generally, β-phase titanium is the more ductile phase and the α-phase is more stress resistant but less tolerable to ductility due to the larger number of slip planes in the bcc structure of the β-phase relative to the hcp α-phase. Consequently, cracks preferentially propagate along the α-phase, as shown in Fig. 6(b).

For a detailed analysis, other surfaces of the fractured tensile specimens were observed along the TD plane. The corresponding SEM images are exhibited in Fig. 7. The Ti-Al intermetallic compound specimen shows a brittle fractured surface with transgranular + cleavage fractures (Fig. 7(a)). The Ti-V-Al ($\alpha + \beta$) alloy specimen reveals a quasi-cleavage fractured surface with a bamboo-like structure; the thickness between the two bamboo ridges is approximately 0.8–4 μm (Fig. 7(b)) [23]. These distances originate from the intergranular fracture along the relatively low ductile α-phase. Therefore, the major reasons for the lowered mechanical properties of the post-heat treated Ti-Al intermetallic compound seen in Fig. 5(a) are considered as: i) existence of voids, ii) larger grain growth, and iii) brittle Ti-Al intermetallic phase. For the Ti-V-Al ($\alpha + \beta$) alloy, it can be regarded that the lamellar structure of the $\alpha + \beta$ phases delays propagation of the cracks, leading to an increase of both UTS and EL, as shown in Fig. 5(b).

The reduced mechanical properties of the Ti-V-Al alloys with increasing Al infiltration time, as observed in Fig. 5(b), were analyzed in terms of their microstructural changes. The SEM images of the Ti-V-Al specimens prepared with infiltration times of 10 and 15 s are displayed in Fig. 8(a) and (b), respectively, and their fractured surfaces along the TD plane are shown in Fig. 8(c) and (d), respectively. As seen in Fig. 8(a) and (b), with increasing infiltration time, the phase constitution in the Ti-V-Al alloys become inhomogeneous and the lamellar region becomes smaller. Consequently, lamellar structures are almost absent at an Al infiltration time of 15 s (Fig. 8(b)). This indicates that the Al infiltration time is crucial to the formation of a lamellar structure in Ti-V-Al alloys. The absence of a lamellar structure in the Ti-V-Al alloys precludes formation of the bamboo-like structured fracture surface; instead a

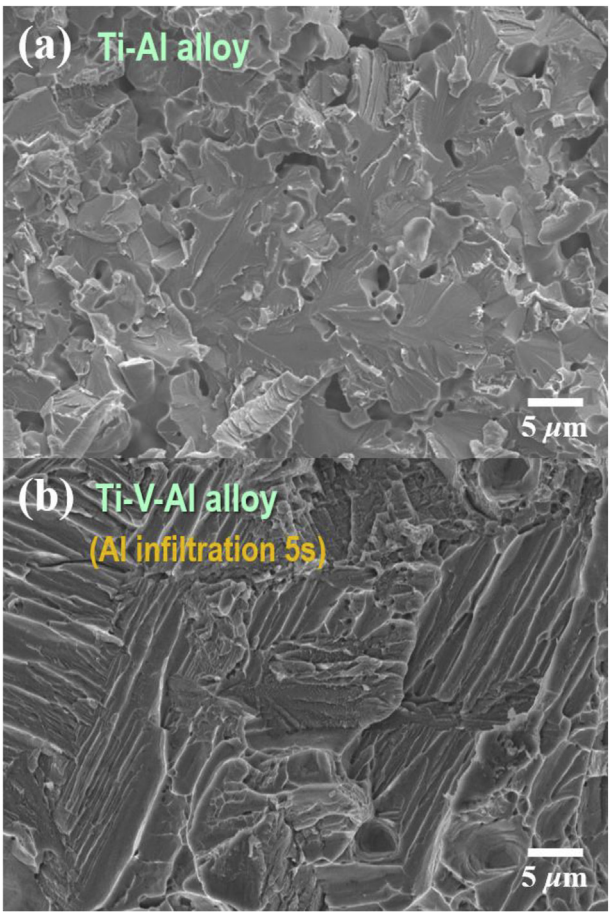

Fig. 7. SEM images of the fractured surface of Ti-V-Al alloys prepared with different infiltration times of (a) 10 and (b) 15 s, which were observed at the tensile direction.

brittle fracture surface is formed, as in the Ti-Al intermetallic compounds (Fig. 8(d)). This can be attributed to a greater aluminum content than that required to form a well-defined $\alpha + \beta$ phase, because of the relatively long infiltration time. The large amount of infiltrated Al promotes formation of brittle Ti-Al intermetallic phases in the Ti-V-Al alloys, resulting in a deterioration of mechanical properties. Therefore, the microstructural results on the increase of infiltration time demonstrate that the lamellar structure of the $\alpha + \beta$ phases delays crack propagation.

In our previous work, the mechanical properties of Ti-Al intermetallic composites were improved by simply adding Mg, whereby molten Al-Mg was infiltrated into porous Ti compacts. As the duration time for Al infiltration increased to 90 s, the mechanical properties of the sample were increased. In this study, the duration time is shortened to just 5 s by using vanadium as the phase stabilizer. Meanwhile, the post-heat treatment process produced adverse effects on the mechanical properties of the Ti-Al alloy due to the formations of brittle intermetallic phases and many voids. However, the post-heat treatment process was beneficial to the mechanical properties of the Ti-V-Al alloy because it strengthened the $\alpha + \beta$ phases. Therefore, a simple and effective route to fabricate Ti-based materials with good mechanical properties has been demonstrated.

4. Conclusions

We effectively combined powder injection molding (MIM) and aluminum infiltration to fabricate reinforced titanium $\alpha + \beta$ alloys. The porous Ti or Ti-V compacts were prepared by MIM and the pores of the Ti or Ti-V compacts were filled with molten Al for various seconds. In the case of the vanadium-free specimens, a brittle intermetallic compound was formed after post-heat treatment, and the mechanical properties were drastically reduced by

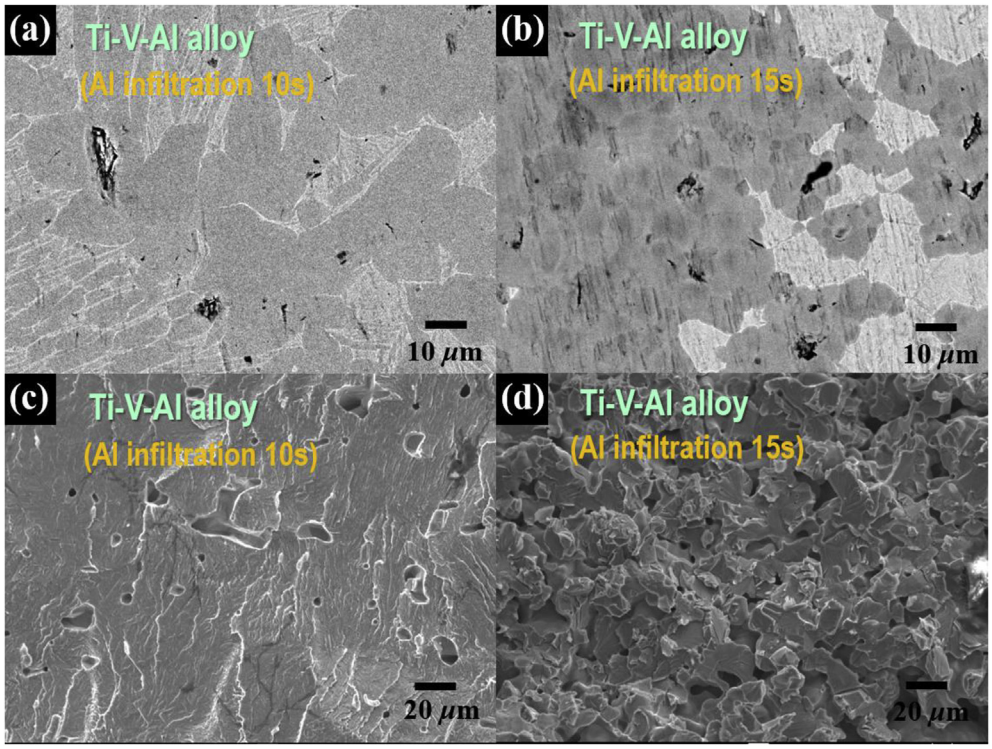

Fig. 8. SEM images of specimens ((a)–(b)) and their fractured surfaces ((c)–(d)) of Ti-V-Al alloys prepared with different infiltration times of 10 and 15 s.

the presence of many voids and large grain size. The vanadium-added specimens, by comparison, showed that an appropriate amount of aluminum and heat treatment stimulates the formation of an $\alpha + \beta$ lamellar structure which has the distinctive feature of enhancing the material's mechanical properties. In other words, by a simple, short, and economically efficient process involving Al pore infiltration and heat treatment, a remarkably enhanced ultimate tensile strength (UTS ~ 697 MPa) and elongation (EL ~ 7.39%) of the resultant Ti $\alpha + \beta$ alloys with near-net shape were obtained.

Acknowledgements

This work was supported by the Priority Research Centers Program(2009-0093823) through the National Research Foundation of Korea (NRF).

References

[1] C. Leyens, M. Peters, Titanium and Titanium Alloys, WILEY-VCH, 2001.
[2] M.T. Jovanovic, S. Tadic, S. Zec, Z. Miskovic, I. Bobic, The effect of annealing temperatures and cooling rates on microstructure and mechanical properties of investment cast Ti-6Al-4V alloy, Mater. Des. 27 (2006) 192–199.
[3] M. Bermingham, S. McDonald, M. Dargusch, D. StJohn, Microstructure of cast titanium alloys, Mater. Forum 31 (2007) 84–89.
[4] Materials Properties Handbook: Titanium Alloys, ASM International, 1994, pp. 483–636.
[5] S.L. Semiatin, V. Seetharaman, I. Weiss, The thermomechanical processing of alpha/beta titanium alloys, J. Met. 49 (1997) 33.
[6] R. Pederson, O. Babushkin, F. Skystedt, R. Warren, The use of high temperature X-ray diffractometry to study phase transitions in Ti-6Al-4V, in: Titanium Alloys at Elevated Temperature: Structure Development and Service Behavior, Institute of Materials, London, 2001. ISSN 1336-5510.
[7] M.A. Khan, R.L. Williams, D.F. Williams, The corrosion behaviour of Ti-6Al-4V, Ti-6Al-7Nb and Ti-13Nb-13Zr in protein solutions, Biomaterials 20 (1999) 631–637.
[8] G. Lütjering, J.C. Williams, Titanium, Springer, Germany, 2003, pp. 227–229.
[9] M.T. Jia, D.L. Zhang, B. Gabbitas, J.M. Liang, C. Kong, A novel Ti–6Al–4V alloy microstructure with very high strength and good ductility, Scr. Mater. 107 (2015) 10–13.
[10] J.D. Paramore, Z.Z. Fang, P. Sun, M. Koopman, K.S. Ravi Chandran, M. Dunstan, A powder metallurgy method for manufacturing Ti-6Al-4V with wrought-like microstructures and mechanical properties via hydrogen sintering and phase transformation (HSPT), Scr. Mater. 107 (2015) 103–106.
[11] F. Cao, K.S. Ravi Chandran, P. Kumar, New approach to achieve high strength powder metallurgy Ti-6Al-4V alloy through accelerated sintering at β-transus temperature and hydrogenation-dehydrogenation treatment, Scr. Mater. 130 (2017) 22–26.
[12] Z. Zhao, J. Chen, H. Tan, G. Zhang, X. Lin, W. Huang, Achieving superior ductility for laser solid formed extra low interstitial Ti-6Al-4V titanium alloy through equiaxial alpha microstructure, Scr. Mater. 146 (2018) 187–191.
[13] K. Faller, F.H. Froes, The use of titanium in family automobiles: current trends, JOM 53 (2001) 27.
[14] Sumin Kim, Gyeungho Kim, Wooyoung Lee, Hyun-Sook Lee, Wonyoung Jeung, A novel method to fabricate reinforced Ti composites by infiltration of Al (Mg) into porous titanium, J. Alloys Compd. 715 (2017) 404–412.
[15] A.Y. Fasasi, S. Mwenifumbo, N. Rahbar, J. Chen, M. Li, A.C. Beye, C.B. Arnold, W.O. Soboyejo, Nano-second UV laser processed micro-grooves on Ti6Al4V for biomedical applications, Mater. Sci. Eng. C 29 (2009) 5–13.
[16] M. Ahmadi, Y. Karpat, O. Acar, Y.E. Kalay, Microstructure effects on process outputs in micro scale milling of heat treated Ti6Al4V titanium alloys, J. Mater. Process. Technol. 252 (2018) 333.
[17] J.D. Cotton, R.D. Briggs, R.R. Boyer, S. Tamirisakandala, P. Russo, N. Shchetnikov, J.C. Fanning, State of the art in beta titanium alloys for airframe applications, JOM 67 (2015) 1281–1303.
[18] Lothar W. Meyer, Lutz Krüger, Kristin Sommer, Thorsten Halle, Matthias Hockauf, Dynamic strength and failure behavior of titanium alloy Ti-6Al-4V for a variation of heat treatments, Mech. Time-Dependent Mater. 12 (2008) 237–247.
[19] Seong-Tak Oh, Kee-Do Woo, Tack Lee, Hae-Cheol Lee, Effects of heat treatment on mechanical properties of VAR-cast Ti-6Al-4V alloy, MCM (2015) 344.
[20] B.D. Venkatesh, D.L. Chen, S.D. Bhole, Effect of heat treatment on mechanical properties of Ti–6Al–4V ELI alloy, Mater. Sci. A Struct. 506 (2009) 117–124.
[21] Reham Reda, Adel A. Nofal, Abdel-Hamid A. Hussein, Effect of quenching temperature on the mechanical properties of cast Ti-6Al-4V alloy, J. Metall. Eng. (2013) 2.
[22] Tatsuro Morita, Kei Hatsuoka, Takashi Iizuka, Kazuhiro Kawasaki, Strengthening of Ti–6Al–4V alloy by short-time duplex heat treatment, Mater. Trans. 46 (2005) 1681–1686.
[23] Seo Yeon Jo, Jeongho Han, Joo-Hee Kang, Singon Kang, Sukjin Lee, Young-Kook Lee, Relationship between grain size and ductile-to-brittle transition at room temperature in Fe–18Mn–0.6C–1.5Si twinning-induced plasticity steel, J. Alloys Compd. 627 (2015) 374–382.